DYNAMIC FAILURE OF CLAMPED CIRCULAR PLATES SUBJECTED TO AN UNDERWATER SHOCK

Sohrab Kazemahvazi, Darren Radford, Vikram S. Deshpande
and Norman A. Fleck

DYNAMIC FAILURE OF CLAMPED CIRCULAR PLATES SUBJECTED TO AN UNDERWATER SHOCK

SOHRAB KAZEMAHVAZI, DARREN RADFORD, VIKRAM S. DESHPANDE AND NORMAN A. FLECK

Clamped circular copper plates have been subjected to exponentially decaying underwater blast waves with peak pressures in the range 10 MPa to 300 MPa and decay constants varying between 0.05 ms to 1.1 ms. The deformation and failure modes were observed by high-speed photography. For the thin plates considered in this study, the failure modes were primarily governed by the peak pressures and were reasonably independent of the blast wave decay constant. Three modes of deformation and failure were identified. At low pressures, the plates undergo bending and stretching without rupture (mode I). At intermediate pressures a range of tensile tearing modes were observed, from petalling failures to tearing at the supports with increasing blast pressures. These tearing modes are referred to as mode II failures. At the highest pressures investigated here, the plate tears at the supports in a manner that is reminiscent of a *shear-off* failure. This failure is labeled as mode III. Scanning electron micrographs of the failure surfaces showed that in all cases, the local failure mechanism was tensile necking. Finite element (FE) simulations employing a local shear failure criterion are used to model the rupture of the material. Appropriately calibrated FE models capture all failure modes with sufficient fidelity.

1. Introduction

Military and commercial ship structures require adequate strength and ductility to survive an underwater explosion. This need has stimulated considerable recent interest in investigating the underwater blast response of metallic monolithic and sandwich structures, see for example [Fleck and Deshpande 2004; Xue and Hutchinson 2003]. Local failure of these metallic structures under dynamic loading is a major design constraint: typically, failure occurs at the supports or at the junction between the sandwich core and faces of a sandwich structure [Radford et al. 2005; Rathbun et al. 2006].

Recent assessments of steel sandwich panels subject to underwater blast exemplify the tendency for rupture at the supports [Liang et al. 2006]. Shortly after arrival of the pressure wave, much of the wet face acquires an uniform velocity. However, small portions of the wet face remain stationary: at the supports, and at the attachment points to the core. Plastic strains concentrate within the wet face adjacent to these stationary locations. Rupture occurs when the plastic strain reaches a critical value (say 20%), causing the wet face to tear.

Experiments on impulsively loaded clamped beams have revealed a range of deformation and failure modes [Menkes and Opat 1973; Nurick and Shave 2000]. At low value of impulse I, the beams plastically bend and stretch without rupture (mode I). At intermediate I, plate stretching is followed by tensile rupture at the supports (mode II). And at high I, shear failure occurs at the supports with negligible plastic deformation in the remainder of the beam (mode III).

Recent theoretical studies by Lee and Wierzbicki [2005a; 2005b] have analyzed the so-called disc-ing and petalling failure modes in impulsively loaded clamped plates. These tensile tearing modes are reminiscent of the mode II failure modes for impulsively loaded beams. On the other hand, Balden and Nurick [2005] have reported an experimental and numerical investigation into the so-called shear rupture modes (mode III) of impulsively loaded clamped circular plates. Systematic experimental studies, along with appropriate high speed photography, are required to elucidate the deformation modes and the range of failure mechanisms of dynamically loaded clamped plates.

The primary aims of this study are:

(i) to investigate the sensitivity of failure mode of monolithic plates to the level of underwater blast pressure and to the decay time of the blast waves.

(ii) to determine the ability of finite element (FE) calculation to predict the observed failure modes.

We report a combined experimental and numerical study on the failure modes of clamped copper plates subjected to an underwater blast. In Section 2 the experimental method is described, based on the underwater shock simulator of [Deshpande et al. 2006]. The observed failure mechanisms are elucidated by high-speed photography, and are discussed in Section 3. The observed failure modes are then used to construct failure regime maps for the clamped copper plates. A limited set of finite element simulations of the failure of the copper plates are reported in Section 4 and are compared with observation.

2. Experimental protocol

2.1. *Summary of the water shock tube apparatus and the Taylor fluid-structure interaction analysis.*
Deshpande et al. [2006] have developed a shock simulator for the underwater shock loading of materials and test structures within the laboratory. The tube is capped at one end by the test structure and by a piston at the other end. The piston is struck by a steel projectile, as sketched in Figure 1. Pressure pulses that decay exponentially with time t are generated in the water. Similar to realistic underwater blasts, these pulses have the form

$$p = p_o e^{-t/\theta}, \tag{1}$$

where p_o is the peak pressure and θ is the decay constant. The apparatus is capable of generating peak pressures in the range 10–300 MPa with decay times ranging from 0.05 ms to 1.5 ms. The peak pressure and the decay time are adjusted independently by varying the projectile velocity and mass, respectively. In particular, using one-dimensional linear wave theory, Deshpande et al. [2006] have shown that (p_o, θ) are related to the projectile mass per unit area m_p and velocity v_o by

$$p_o = \rho_w c_w v_o \tag{2a}$$

and

$$\theta = \frac{m_p}{\rho_w c_w}, \tag{2b}$$

where ρ_w is the density of water and c_w is the speed of sound in water. Good agreement was observed between the measured pressure pulses and these simple analytical predictions.

In the present study, a water shock tube is used to load a clamped circular copper plate of mass per unit area m_f. The momentum transmitted to the plate can be estimated using the one-dimensional fluid-structure interaction analysis of [Taylor 1941] for an underwater pressure pulse of the form of Equation
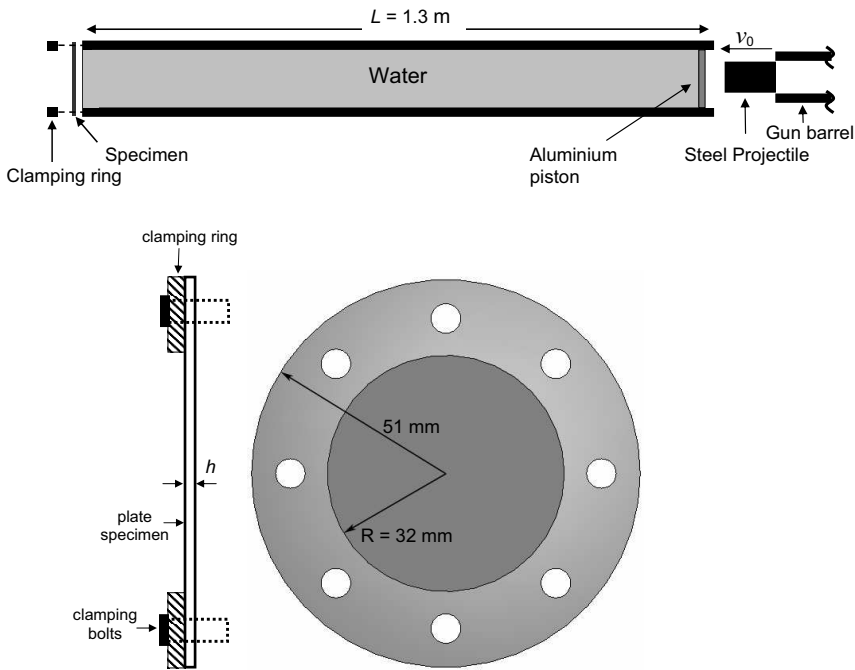
Figure 1. Schematic of the water shock tube experimental set-up, not to scale (above). Sketch of the copper plate test specimen along with the side view of the clamping arrangement (below).

(1) impinging on a free standing plate. When this pressure wave hits a stationary rigid plate at normal incidence, it imparts an impulse

$$I_o = 2 \int_0^\infty p_o e^{-t/\theta} dt = 2p_o \theta \tag{3}$$

to the plate. The factor of two arises in Equation (3) due to full reflection of the pressure wave. If, instead, the pressure wave impacts a free-standing plate, the imparted impulse is less than I_o, and can be estimated as follows. When the pressure wave strikes a free standing plate, it sets the plate in motion and is partly reflected. Cavitation of the water occurs when the pressure at the interface between the plate and the fluid drops to zero; this occurs a time τ_c after initial impingement given by

$$\frac{\tau_c}{\theta} = \frac{1}{\psi - 1} \ln \psi, \tag{4}$$

where $\psi \equiv \rho_w c_w \theta / m_f$. The momentum per unit area I_{trans} transmitted into the plate up to the instant of cavitation is given by

$$I_{\text{trans}} = I_o \zeta, \tag{5a}$$

where

$$\zeta \equiv \psi^{\psi/(1-\psi)}. \tag{5b}$$

We shall investigate the failure modes of the clamped plate as a function of both the peak blast wave pressure p_o and the Taylor fluid-structure interaction parameter ψ.

2.2. *Specimen configuration.* Clamped circular copper plates of diameter 102 mm and thicknesses $h = 0.08$ mm and 0.25 mm were tested using the water shock tube sketched in Figure 1. Eight equally spaced clearance holes for M8 bolts were drilled into the copper plates on a pitch circle of radius 41 mm, to enable clamping of the copper plate onto the end the water tube (Figure 1). To facilitate this an annular steel ring was used, of thickness 10 mm, inner radius 32 mm, and outer radius 51 mm. Thus, the effective radius of the clamped plate was $R = 32$ mm.

The water column is located in a steel tube of length $L = 1.3$ m, internal diameter $\phi = 64$ mm and wall thickness $w = 19$ mm. The tube is capped at one end by a 6 mm thick aluminum piston and at the opposite end by the copper specimen. The piston has an O-ring seal and contains a bleed valve to ensure that air is not trapped in the water column, as detailed by Deshpande et al. [2006]. Dynamic loading is achieved by firing steel circular cylinders of diameter $d = 28.5$ mm and mass in the range 0.2 kg to 5 kg at the piston of the water tube. The water tube is aligned such that the projectile strikes the piston centrally and normally. The projectiles are accelerated using a gas gun of barrel length 4.5 m and inner diameter 28.5 mm. No sabot is employed and bursting of copper shim diaphragms forms the breach mechanism of the gas gun. The projectile velocity ranges from $10 \, \mathrm{ms}^{-1}$ to $180 \, \mathrm{ms}^{-1}$, measured at the exit of the barrel using laser-velocity gates. The pressure transient in the water tube was measured using a high frequency piezoelectric pressure sensor. This pressure transducer, with an in-built charge amplifier, is specifically designed for shock tube and blast wave measurements. It has a dynamic measurement range of 0 to 300 MPa, a rise time of less than 1 μs, and a resonant frequency above 500 kHz.

2.3. *Test protocol.* As discussed in Section 2.1 above, the peak pressure and the decay time of the pressure transients in the shock tube were controlled by varying the projectile velocity and mass, respectively. Experiments were designed to span a range of peak pressures p_o and fluid-structure interaction parameter ψ for each plate thickness. High-speed photographic sequences of the dry face of the copper plates were taken using a Hadland 790 camera, thereby allowing for direct observation of the sequence of deformation and failure modes of the plates.

2.4. *Material properties.* The uniaxial tensile response of the copper used to manufacture the circular plate specimens was measured at a nominal strain rate of $10^{-3} \, \mathrm{s}^{-1}$, and the true tensile stress versus logarithmic plastic strain curve is plotted in Figure 2. We denote this curve by $\sigma_0(\varepsilon^p)$. The measured 0.2% offset yield strength σ_Y was 220 MPa, and ultimate tensile strength $\sigma_{UTS} = 320$ MPa occurred at a tensile failure strain $\varepsilon_f \approx 22\%$.

Lindholm [1964] investigated the sensitivity of the stress-strain response of copper to plastic strain rate $\dot{\varepsilon}^p$ over the range $10^{-3} \, \mathrm{s}^{-1} < \dot{\varepsilon}^p < 10^4 \mathrm{s}^{-1}$. Their data suggest that the dynamic strength σ_d versus plastic strain ε^p of the copper used in the present study can be written in the form

$$\sigma_d(\varepsilon^p) = q(\dot{\varepsilon}^p) \, \sigma_0(\varepsilon^p), \tag{6}$$

where $\sigma_0(\varepsilon^p)$ is the uniaxial stress-strain curve of the present investigation at $\dot{\varepsilon}^p = 10^{-3} \mathrm{s}^{-1}$, as plotted in Figure 2. The multiplying factor $q(\dot{\varepsilon}^p)$ denotes the ratio of the stress at an applied strain-rate $\dot{\varepsilon}^p$ to the stress at an applied strain rate $\dot{\varepsilon}^p = 10^{-3} \, \mathrm{s}^{-1}$. The stress versus strain histories measured by Lindholm
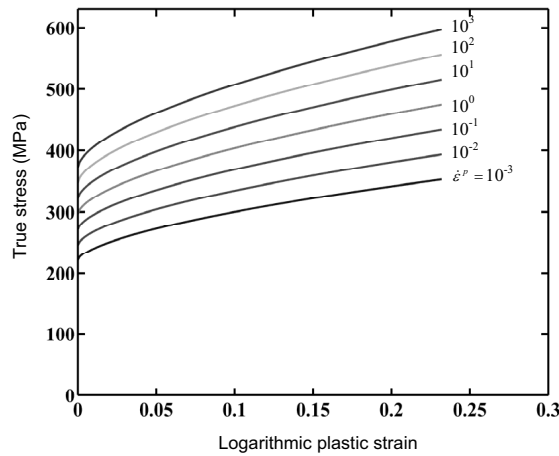
Figure 2. Measured uniaxial tensile response of the copper at an applied plastic strain rate $\dot{\varepsilon}^p = 10^{-3}\,\mathrm{s}^{-1}$. Estimated tensile stress versus strain histories for the copper at selected higher values of the applied strain-rate are also included using data from [Lindholm 1964].

[1964] indicate that q is reasonably independent of the magnitude of plastic strain ε^p. The estimates in Equation (6) of true tensile stress versus logarithmic plastic strain at selected values of $\dot{\varepsilon}^p$ are included in Figure 2.
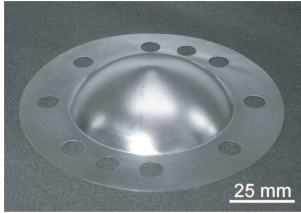
3. Summary of experimental findings

Results are described in detail for the $h = 0.25\,\mathrm{mm}$ copper plates subjected to water blasts with a decay constant $\theta = 0.05\,\mathrm{ms}$ (Taylor fluid-structure interaction parameter $\psi = 31$). Subsequently, we compare these findings with those for other values of ψ and for the $h = 0.08\,\mathrm{mm}$ plate.

3.1. *Failure modes of the $h = 0.25\,mm$ with $\psi = 31$.* Post-test photographs of the $h = 0.25\,\mathrm{mm}$ copper plates are shown in Figure 3. These specimens were subjected to water blasts of decay constant $\theta = 0.05\,\mathrm{ms}$ and a range of peak pressures p_o. The deformation and failure modes are subdivided into three modes, consistent with the classification system of [Menkes and Opat 1973].

At low blast pressures ($p_o \leq 35\,\mathrm{MPa}$), the plate undergoes plastic bending and stretching but no failure is observed (Figure 3a). This is the dishing mode, and is referred to as *mode I*. High speed photography revealed that the deformation mode involves plastic hinges traveling from the periphery to the center of the plate, followed by stretching and bending of the plate in a manner similar to the quasistatic deformation mode of a clamped circular plate under uniform transverse pressure. This deformation history supports several theoretical predictions [Wang and Hopkins 1954; Florence 1966].

At intermediate blast pressures, a variety of tensile failure modes of the plates are triggered (Figure 3b). These are labeled as *mode II* failures, wherein the plates assume a dome-shaped final profile with failure at the center and/or periphery. In particular, the following modes were observed:

(a) Mode I   (b) Mode II   (c) Mode III

$p_0 = 34$ MPa ($w_B = 16.8$ mm)

$p_0 = 64$ MPa

$p_0 = 88$ MPa

$p_0 = 130$ MPa

$p_0 = 137$ MPa

$p_0 = 173$ MPa

Figure 3. Post-test photographs of the $h = 0.25$ mm copper plates subjected to $\theta = 0.05$ ms water blasts for a range of peak pressures p_o. The deformation and failure modes have been divided into three modes motivated by the classification system introduced by Menkes and Opat [1973]. The final mid-span deflection of the plate in mode I is marked for (a).

(i) at $p_o = 64$ MPa, the plate fails by the formation of four petals. We shall show subsequently that this failure is initiated by the onset of tearing at the center of the plate;

(ii) with increasing blast pressure, failure initiates at the center of the plate but the petals do not fully develop. Tearing at the supports intervenes (110 MPa $< p_o < 120$ MPa);

(iii) at higher pressures (130 MPa $< p_o < 135$ MPa) the plate tears at the inner periphery of the annular clamps, with no failure at the center of the plate.

For the highest pressures investigated here ($p_o \geq 137$ MPa), the plate tears off the supports before the traveling hinges have reached the center of the plate, and the final deformed shape of the plates resembles a flat-topped dome with failure at the periphery (Figure 3c). This mode is reminiscent of the *shear-off mode III* as identified by Menkes and Opat [1973]. Here we arbitrarily define mode III failures as those cases where the plates cleanly tears at the supports with the traveling hinges not reaching the mid-span of the plate, giving rise to the flat-topped final deformed profiles of the plates (Figure 3c).

3.2. *High speed photographic sequences of the failure modes for the $h = 0.25$ mm plates with $\psi = 31$.* High speed photographic sequences of the deformation and failure modes of the plates are included

in Figures 4–6 for increasing values of the blast pressure p_o. In each of the photographic sequences traveling hinges initiate at the supports and travel towards the mid-span of the plate. At $p_o = 64$ MPa (Figure 4), a mode II failure initiates at the mid-span immediately after the traveling hinges coalesce there. Petalling of the plates is evident, with the resulting outburst of the water. In Figure 5 ($p_o = 130$ MPa), we observe that the plate tears off from the supports prior to the traveling hinges reaching mid-span. Note that wrinkling of the plates near the supports at $t = 50\,\mu$s indicates that the plate has detached from the supports. However, the hinges continue to travel towards the mid-span after the plate has separated from the supports, as evidenced by the photographs for $t > 50\,\mu$s and the final deformed shape. For this level of blast pressure the plate only acquires a uniform velocity after the traveling hinges have coalesced at mid-span. At a blast pressure $p_o = 173$ MPa (Figure 6), the plate again tears from the supports at $t = 50\,\mu$s. After circumferential tearing has completed, the hinges remain very close to the supports, and the plate acquires a final, spatially uniform velocity. The final deformed shape of the plate is reminiscent of the shear-off mode III of [Menkes and Opat 1973].

3.3. *Examination of fracture surfaces.* The plates failed either at mid-span after coalescence of traveling plastic hinges or at the supports. The macroscopic failure modes are shear-off near the supports and petalling by tensile necking. It is instructive to determine whether the microscopic mode of failure (tension versus shear) is the same as that suggested by the macroscopic mode. In order to address this, scanning electron micrographs of the failure surfaces of the plates subjected to blast pressures $p_o = 64$ MPa and 173 MPa ($\psi = 31$) are shown in Figures 7 and 8, respectively. It is concluded from the micrographs that the local failure mechanism is tensile necking, regardless of whether the macroscopic mode is petalling (at $p_o = 64$ MPa) or shear-off ($p_o = 173$ MPa). We conclude that the thin copper plates fail by local tensile necking over the entire range of blast pressures considered.

3.4. *Failure mechanism maps.* Consider a clamped circular plate of radius R and thickness h made from a rigid, ideally plastic material of yield strength σ_Y and density ρ_f. This plate is subjected to a spatially uniform underwater blast of the form of Equation (1). Following Fleck and Deshpande [2004] we can argue that the response can be temporally decoupled into two stages. First, in a fluid-structure interaction phase, the plate acquires a momentum I_{trans} as given by analysis of [Taylor 1941]. Subsequent loading by the water is neglected and the second phase of the response reduces to the classical problem of an impulsively loaded clamped plate as analyzed (for small deflections) by Wang and Hopkins [1954]. The relevant nondimensional groups governing the deformation of the plate are

  (i) the aspect ratio of the plate $\frac{R}{h}$, and

  (ii) the nondimensional transmitted impulse $\frac{I_{\text{trans}}}{(h\sqrt{\rho_f \sigma_Y})}$.

For the large values of ψ considered in this study, the Taylor estimate (Equation (5)) for the transmitted impulse reduces to

$$I_{\text{trans}} \approx \frac{2\rho_f h p_o}{\rho_w c_w}, \tag{7}$$

independent of the value of θ. This suggests that the deformation and failure of the plates are only dependent on the peak pressure of the blast p_o and independent of the decay constant θ. We shall gauge the validity of this prediction by experimentally probing the failure modes of the plates for a decay constant in the range $0.05\,\text{ms} \le \theta \le 1.1\,\text{ms}$.

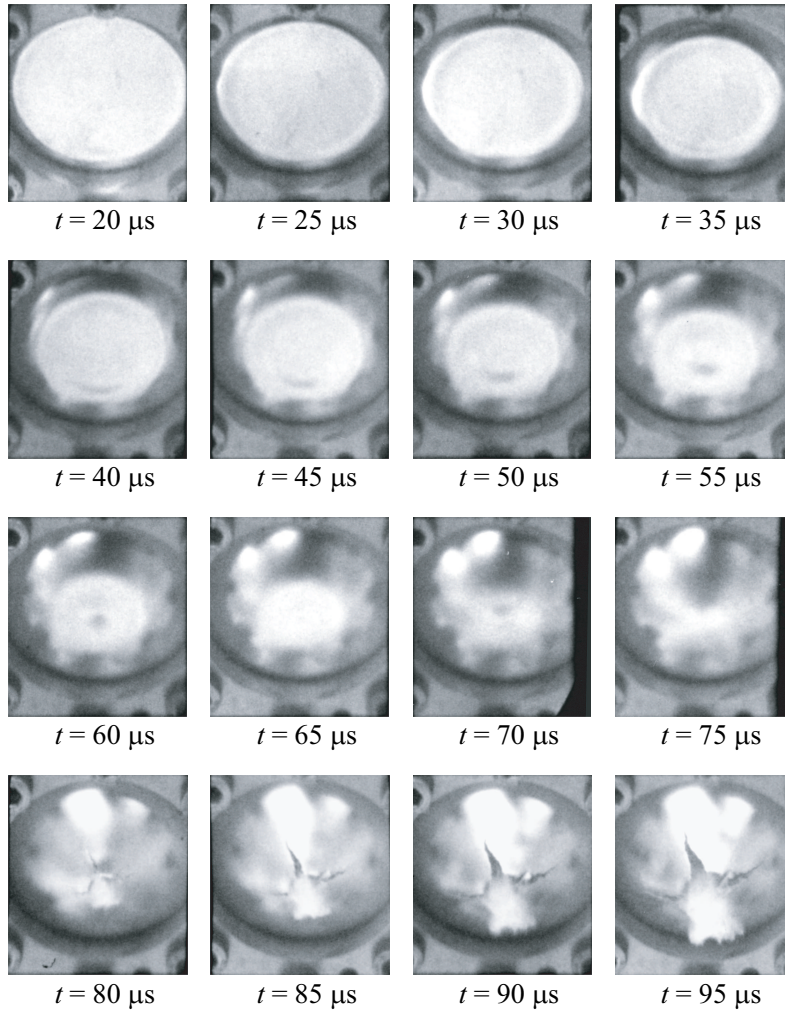**Figure 4.** High-speed photographic sequence (exposure time $4\,\mu$s) of the $h = 0.25$ mm copper plate subjected to a blast with a peak pressure $p_o = 64$ MPa and decay constant $\theta = 0.05$ ms (mode II: petalling failure). Time after the arrival of the shock is indicated for each frame.

The response of the plates can be determined in terms of four independent nondimensional groups: R/h, ρ_f/ρ_w, p_o/σ_{UTS}, and $h/(c_w\theta)$. With ρ_f/ρ_w held fixed in this study we plot maps using axes of the peak blast pressure normalized by the ultimate tensile strength of the copper, p_o/σ_{UTS}, and the normalized plate thickness, $h/(c_w\theta)$, for two values of R/h corresponding to the $h = 0.25$ mm and 0.08 mm plates investigated here. The observed failure modes of the copper plates are summarized in maps in Figure 9 for the $h = 0.25$ mm ($R/h = 128$) and 0.08 mm ($R/h = 400$) plates, respectively. The maps were generated as follows. For each plate thickness, experiments were performed for a fixed value of θ and increasing values of p_o. The failure modes (according to the classification system of Section 3.1) were determined by post-test examination of the specimens. The procedure was repeated for selected

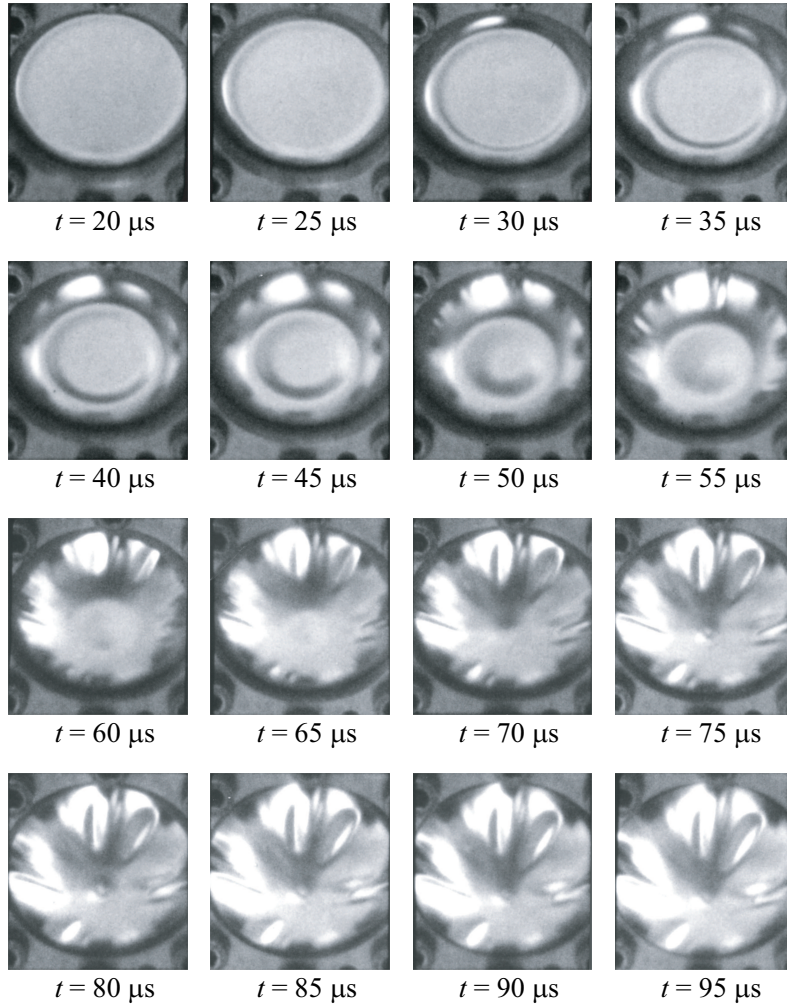**Figure 5.** High-speed photographic sequence (exposure time $4\,\mu$s) of the $h = 0.25$ mm copper plate subjected to a blast with a peak pressure $p_o = 130$ MPa and decay constant $\theta = 0.05$ ms (mode II: support failure). Time after the arrival of the shock is indicated for each frame.

values of the decay constant θ for each plate thickness. The boundaries between the modes are included on the figures.

The following deductions are made from the failure mechanism maps:

 (i) For both plate thicknesses and for all values of θ considered here, the failure mode switches from mode I through to mode III with increasing p_o.

 (ii) In line with the expectations outlined at the beginning of Section 3.4, the failure modes are primarily a function of the peak pressure p_o, and are only weakly depend upon the value of the wave decay constant; upon increasing θ by nearly two orders of magnitude, the peak pressure to transit from mode II to mode III decreases by only a factor of two.
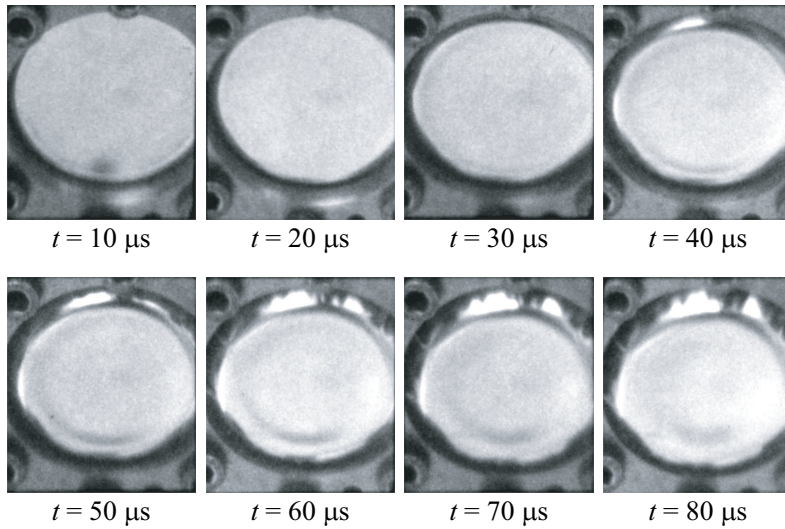
Figure 6. High-speed photographic sequence (exposure time $4\,\mu s$) of the $h = 0.25\,\text{mm}$ copper plate subjected to a blast with a peak pressure $p_o = 173\,\text{MPa}$ and decay constant $\theta = 0.05\,\text{ms}$ (mode III support failure). Time after the arrival of the shock is indicated for each frame.
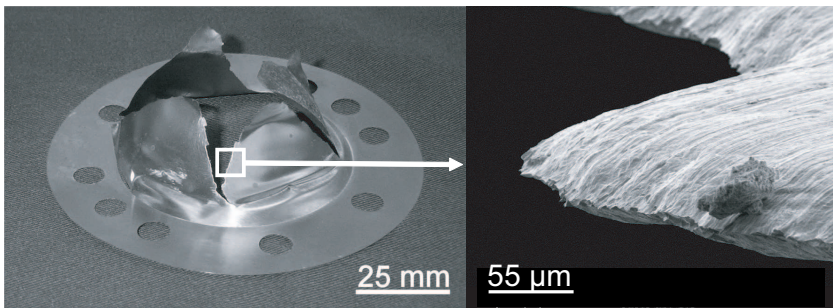

Figure 7. Scanning electronic micrographs of the failed surface of the $h = 0.25\,\text{mm}$ copper plate subjected to a blast with a $p_o = 64\,\text{MPa}$ and decay constant $\theta = 0.05\,\text{ms}$.
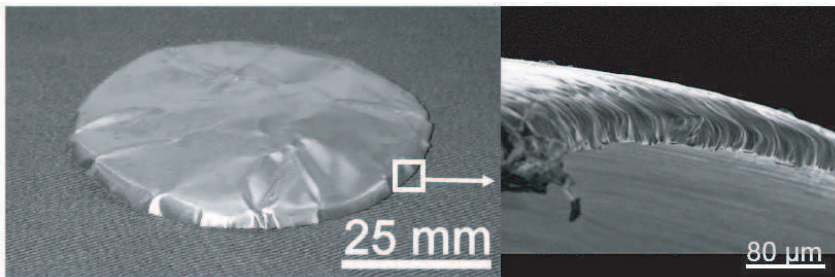

Figure 8. Scanning electronic micrographs of the failed surface of the $h = 0.25\,\text{mm}$ copper plate subjected to a blast with a $p_o = 173\,\text{MPa}$ and decay constant $\theta = 0.05\,\text{ms}$.
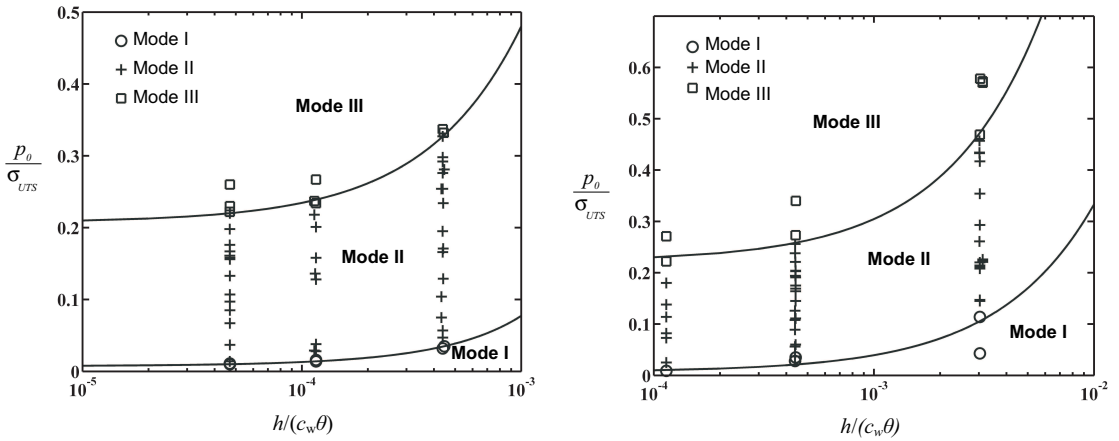
Figure 9. The regimes of dominance of the observed three modes of deformation and failure are indicated on a map of normalized peak pressure and nondimensional plate thickness for the $h = 0.25$ mm ($R/h = 128$) (above) and $h = 0.08$ mm ($R/h = 400$) (below) copper plates.

We also note that the failure mechanism maps for both the plate thicknesses ($R/h = 128$ and 400) are very similar. This suggests that, at least for $R/h \geq 128$, the plate aspect ratio does not significantly affect the failure modes of the copper plates. It is concluded that the blast pressure dictates the operative failure mode.

4. Numerical investigation of the failure modes

We proceed to present a limited numerical investigation into the failure modes of the copper plates. The aim is to determine the capability of a finite element model in capturing the range of failure modes observed in the experiments described above. Attention is restricted to the choice $h = 0.25$ mm subjected to underwater blasts with decay constant $\theta = 0.05$ ms ($\psi = 31$).

4.1. *Finite element model.* Finite element calculations of the response of the clamped plates were performed using the explicit time integration version of the commercial finite element package ABAQUS. The circular plates of radius $R = 32$ mm were modeled using three-dimensional 4-noded quadrilateral shell elements (of type S4R in ABAQUS notation) with 5 integration points through the thickness of the elements. In most of the calculations, the elements were of approximate in-plane dimension $30 \, \mu$m $\times$ $90 \, \mu$m near the center of the plate (57600 elements in total); the effect of mesh size upon the predicted deformation and failure response is discussed below in Section 4.3. The boundary conditions were as follows. The circular plate was clamped along its periphery with all displacement and rotational degrees of freedom constrained to zero. The experimental results presented in Section 3 suggest that it is acceptable to decouple the fluid-structure interaction phase from the stretching and bending phases of the plate response. Hence we did not explicitly model the fluid-structure interaction phase. Instead, the estimate of [Taylor 1941] was employed to determine the blast momentum transmitted into the plate. We

assumed that the blast imparts a spatially uniform velocity

$$v_o = \frac{2 p_o \theta \zeta}{\rho_f h} \tag{8}$$

to the plate. This velocity was applied as an initial velocity boundary condition to the entire plate and the subsequent deformation and failure were determined by the finite element method.

4.2. *Assumed constitutive description for the copper.* The copper was modelled as a J2-flow theory rate dependent solid of density $\rho_f = 8960\,\text{kgm}^{-3}$, Young's modulus $E = 105\,\text{GPa}$, and Poisson ratio $\nu = 0.34$. The uniaxial tensile true stress versus equivalent plastic strain curves at plastic strain-rates $10^{-3}\,\text{s}^{-1} \leq \dot{\varepsilon}^p \leq 10^4\,\text{s}^{-1}$ were tabulated in ABAQUS using the data of Figure 2. In addition, it was assumed that the copper lost all strength at a material point when the effective plastic strain ε^p attained the tensile failure strain in a quasistatic tension test $\varepsilon_f = 0.22$. For simplicity, this failure strain is assumed to be independent of strain-rate and stress triaxiality[1]. Formally, the failure criterion is expressed in terms of damage parameter ω, defined as

$$\omega = \int\limits_0^t \frac{d\varepsilon^p}{\varepsilon_f}. \tag{9}$$

Failure occurs when $\omega = 1$, whereupon the failed element is deleted from the calculation.

We emphasize that the assumed failure criterion contains no material length, and consequently the predictions of the numerical simulations are inherently mesh-size dependent (see [Needleman and Tvergaard 1994; Gullerud et al. 2000]). The mesh size w, coupled with the failure strain, dictates the amount of localized deformation that occurs on the fracture plane, and the displacement jump across the critical element is analogous to the critical displacement in a cohesive zone formulation. Thus, for an ideally plastic material with a yield strength σ_Y, the intrinsic mode I crack tip toughness K_{IC} is given as $K_{IC} \sim \sqrt{E w \sigma_Y \varepsilon_f}$ (w being the element width), as discussed by Nahshon et al. [2007]. Thus with $w = 90\,\mu\text{m}$ and $\sigma_Y = 220\,\text{MPa}$, this implies that the assumed fracture toughness $K_{IC} \approx 22\,\text{MPa m}^{1/2}$, which is consistent with a wide body of experimental data for copper. In addition to its role in determining toughness, the mesh size governs the resolution of the predicted strain distribution adjacent to the crack tip. Consequently, the selected mesh must be sufficiently fine to ensure adequate strain resolution, yet be of sufficient size to give a realistic toughness.

4.3. *Illustration of mesh size dependence of the failure predictions.* A scoping study of the failure of circular plates subjected to impulsive loads was performed in order to investigate the effect of mesh size on the failure predictions. To simplify the calculations we considered an axisymmetric FE model of a clamped circular copper plate of radius $R = 32\,\text{mm}$ and thickness $h = 0.25\,\text{mm}$. The FE model comprised 2 noded axisymmetric shell elements (SAX1 in the ABAQUS notation), and the element size w was varied from 0.03 mm to 1.0 mm. All degrees of freedom were constrained at the plate periphery at radial distance $r = R$. The plate was given a spatially uniform initial velocity v_o in the axial direction. For a given mesh size w, v_o was increased in steps of $5\,\text{ms}^{-1}$, and the critical velocity v_crit at which failure of the plate at the supports first occurs was determined from the FE calculations.

---

[1]Very low hydrostatic stresses are generated in these thin plates and hence it is considered reasonable to neglect the effect of stress triaxiality on ε_f.
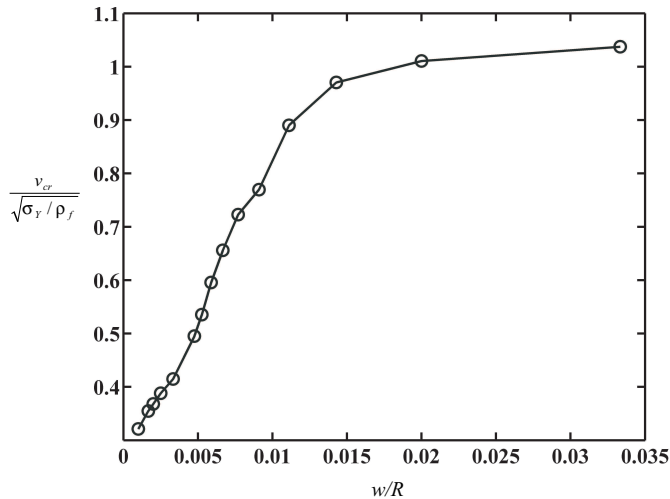
Figure 10. Illustration of the mesh dependence of predictions. Axisymmetric FE predictions of the normalized velocity at which the $h = 0.25$ mm copper plate first fails at the supports as a function of the normalized mesh size.

The normalized critical velocity $v_{\text{crit}}/\sqrt{\sigma_Y/\rho_f}$ is plotted in Figure 10 as a function of the normalized mesh size w/R. Here, $\sigma_Y = 220$ MPa is the quasistatic yield strength of copper. We observe that v_{crit} increases monotonically with increasing w for all mesh sizes investigated here. This is rationalized by recalling that the toughness of the copper in the FE model scales with w. It is emphasized that no independent measurements of the toughness were made in order to determine the appropriate value of w. Rather, we choose a mesh size to ensure agreement with the experimentally observed failure modes over the entire range of pressures investigated here.

4.4. *Numerical results.* We proceed to show comparisons between the FE predictions and experimental observations of the failure of the $h = 0.25$ mm copper plates subjected to an underwater blast with decay constant $\theta = 0.05$ ms ($\psi = 31$). As mentioned above, in the FE calculations, the fluid-structure interaction was not modeled explicitly and the initial velocity, as given by Equation (8), was imparted to the plate for each value of the peak blast pressure p_o.

FE predictions of the time sequences of the deformation of the plates subjected to blast pressures $p_o = 84$ MPa and 170 MPa are given in Figures 11 and 12, respectively. For the choice $p_o = 84$ MPa the calculated failure mode of petalling resembles the observed mode in Figure 5. However, the predicted value of required pressure level for petalling is about 20% higher than the measured value. This discrepancy may be due to: (i) the FE calculations neglect additional fluid loading after first cavitation, and (ii) the failure model employed in the FE calculations overestimates the material toughness at low values of the blast pressures. Moreover, unlike in the experiments, the petals in the FE calculations do not reach the plate periphery. Recall that the element sizes in the FE calculation increases towards the plate periphery, resulting in an increase in the material toughness towards the periphery. Thus, the petals in the FE calculation are arrested at approximately $r = R/2$ in the FE calculations.
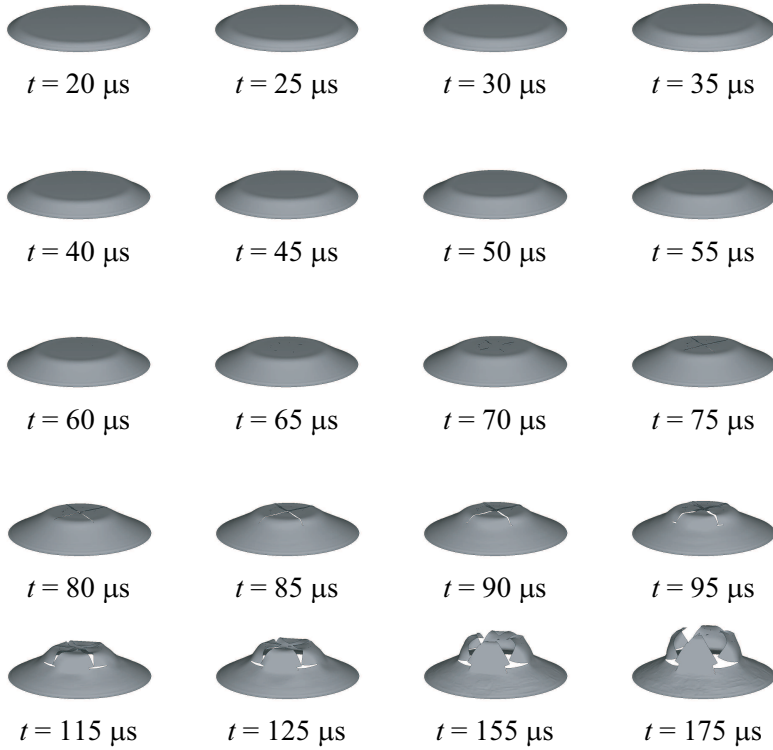
$t = 20\,\mu s$ $t = 25\,\mu s$ $t = 30\,\mu s$ $t = 35\,\mu s$

$t = 40\,\mu s$ $t = 45\,\mu s$ $t = 50\,\mu s$ $t = 55\,\mu s$

$t = 60\,\mu s$ $t = 65\,\mu s$ $t = 70\,\mu s$ $t = 75\,\mu s$

$t = 80\,\mu s$ $t = 85\,\mu s$ $t = 90\,\mu s$ $t = 95\,\mu s$

$t = 115\,\mu s$ $t = 125\,\mu s$ $t = 155\,\mu s$ $t = 175\,\mu s$

Figure 11. FE predictions of the evolution of the deformation and failure of the $h = 0.25$ mm copper plate subjected to a blast with a peak pressure $p_o = 84$ MPa and decay constant $\theta = 0.05$ ms. The petalling failure mode (mode II) similar to the observations (Figure 4) is predicted.

The FE prediction for (mode III) at $p_o = 170$ MPa is in good qualitative agreement with the observed response at $p_o = 173$ MPa; compare Figures 6 and 12. Failure at the periphery of the plate is evident in both cases.

Comparisons between the observed and FE predictions of the final deformed shapes of the copper plates subjected to a range of blast pressures are included in Figure 13. These comparisons indicate that over the whole range of pressures investigated here, reasonable agreement between the observed and FE predictions of failure modes is obtained. It is worth noting that the FE predictions have sufficient fidelity to capture the wrinkling of the plates near the failure surfaces for the $p_o = 125$ MPa and $p_o = 170$ MPa.

5. Concluding remarks

A water shock tube has been employed to investigate the deformation and failure modes of clamped circular copper plates of radius 32 mm and thicknesses 0.08 mm and 0.25 mm. The plates were subjected to blast waves with peak pressures in the range 10 MPa to 120 MPa and decay constants varying between 0.05 ms to 1.1 ms. The deformation and failure modes were observed via high-speed photography.
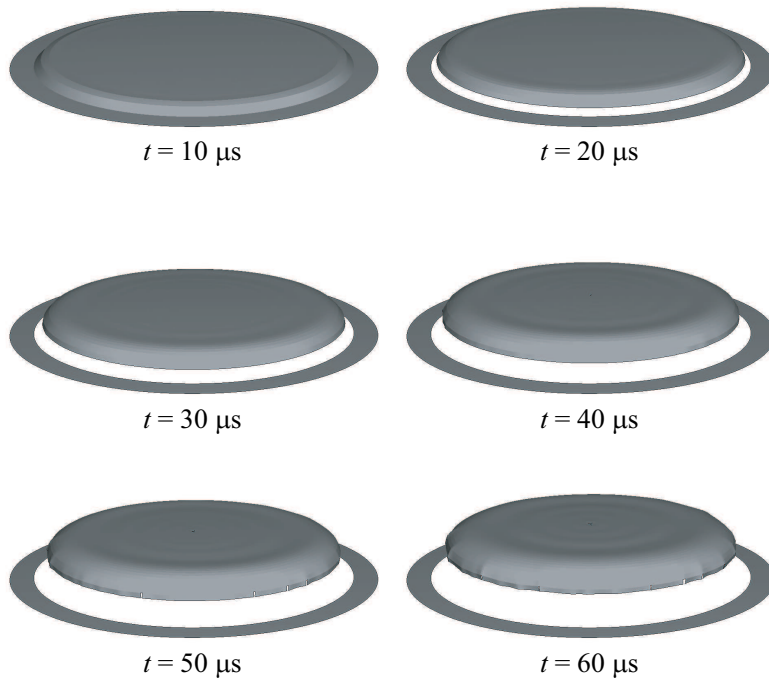
Figure 12. FE predictions of the evolution of the deformation and failure of the $h = 0.25$ mm copper plate subjected to a blast with a peak pressure $p_o = 170$ MPa and decay constant $\theta = 0.05$ ms. Support failure with negligible deformation of the plate (mode III) similar to the observations (Figure 6) is predicted. The clamped portion of the plate is sketched in to clearly illustrate failure.

For the thin plates considered in this study, the failure modes were primarily governed by the peak pressures and were relatively insensitive to the blast wave decay constant. Three modes of deformation and failure were identified. At low pressures, plastic bending and stretching of the plates occurred with no observable failures (mode I). At moderate pressures, the plates assume a dome-shaped final profile with failure at the mid-span and/or periphery. This is termed mode II failure. At the highest pressures investigated here mode III failure occurs: the plate tears at the supports while remaining almost flat. Consequently, the final deformed profile of the plates resembles a flat-topped dome with failure at the periphery. This mode is reminiscent of the shear-off failure reported by Menkes and Opat [1973]. Scanning electron micrographs of the failure surfaces showed that in all cases, the local failure mechanism was tensile necking.

A limited number of finite element (FE) calculations were performed to investigate the fidelity of such simulations to capture the observed deformation and failure modes. A simple critical shear strain failure criterion was employed to model material rupture. As there is no intrinsic length scale in the failure criterion, the simulations are mesh size dependent: the mesh size combined with the material properties dictates the material toughness in such an approach. With an appropriate calibration of the mesh size, the FE calculations captured all the observed failure modes to sufficient fidelity.
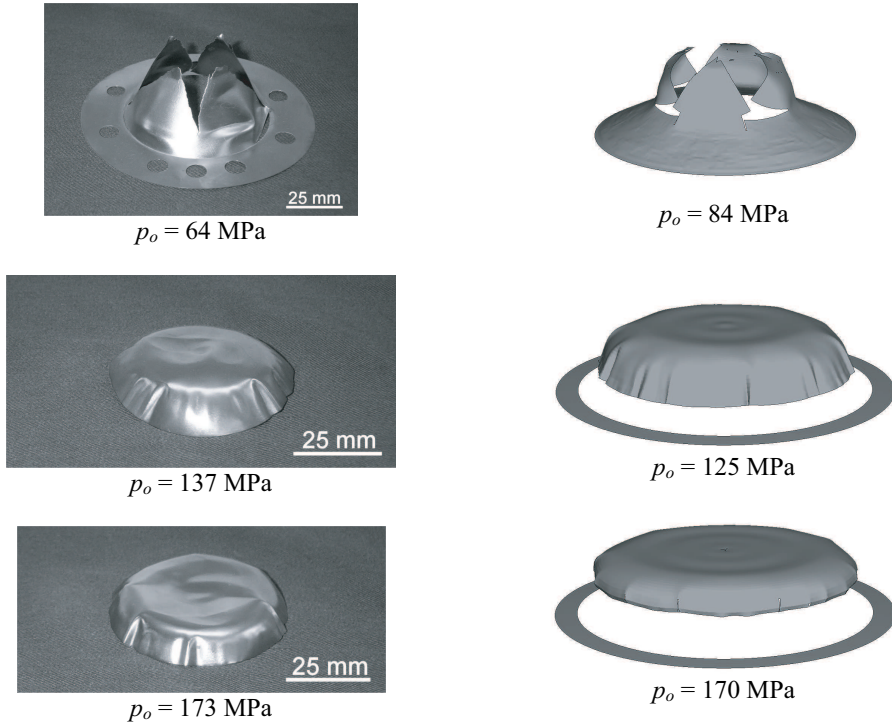
$p_o = 64$ MPa

$p_o = 84$ MPa

$p_o = 137$ MPa

$p_o = 125$ MPa

$p_o = 173$ MPa

$p_o = 170$ MPa

Figure 13. Comparisons between the observed and FE predictions of the final deformed shapes of the $h = 0.25$ mm copper plates subjected to a range of blast pressures with a decay constant $\theta = 0.05$ ms. The clamped portions of the plates are sketched in for the $p_o = 125$ MPa and $p_o = 170$ MPa calculations to clearly illustrate the failure.

Acknowledgements

References

[Balden and Nurick 2005] V. H. Balden and G. N. Nurick, "Numerical simulation of the post-failure motion of steel plates subjected to blast loading", *Int. J. Impact Eng.* **32** (2005), 14–34.

[Deshpande et al. 2006] V. S. Deshpande, A. Heaver, and N. A. Fleck, "An underwater shock simulator", *Proc. R. Soc. Lon. Ser-A* **462** (2006), 1021–1041.

[Fleck and Deshpande 2004] N. A. Fleck and V. S. Deshpande, "Shock resistance of sandwich beams", *J. Appl. Mech. (Trans. ASME)* **71** (2004), 386–401.

[Florence 1966] A. L. Florence, "Circular plate under a uniformly distributed impulse", *Int. J. Solids Struct.* **2** (1966), 37–47.

[Gullerud et al. 2000] A. S. Gullerud, X. Gao, B. Dodds Jr., and R. Haj-Ali, "Simulation of ductile crack growth using computational cells: numerical aspects", *Eng. Fract. Mech.* **66** (2000), 65–92.

[Lee and Wierzbicki 2005a] Y.-W. Lee and T. Wierzbicki, "Fracture prediction of thin plates under localized impulsive loading. part I: dishing", *Int. J. Impact Eng.* **31** (2005a), 1253–1276.

[Lee and Wierzbicki 2005b] Y.-W. Lee and T. Wierzbicki, "Fracture prediction of thin plates under localized impulsive loading. part II: discing and petalling", *Int. J. Impact Eng.* **31** (2005b), 1277–1308.

[Liang et al. 2006] Y. Liang, A. V. Spuskanyuk, S. E. Flores, D. R. Hayhurst, J. W. Hutchinson, R. M. McMeeking, and A. G. Evans, "Response of metallic sandwich panels to water blasts", *J. Appl. Mech.* (*Trans. ASME*) (2006). In Press.

[Lindholm 1964] U. S. Lindholm, "Some experiments with the split Hopkinson pressure bar", *J. Mech. Phys. Solids* **12** (1964), 317–335.

[Menkes and Opat 1973] S. B. Menkes and H. J. Opat, "Tearing and shear failure in explosively loaded clamped beams", *Exp. Mech.* **13** (1973), 480–486.

[Nahshon et al. 2007] K. Nahshon, M. G. Pontin, A. G. Evans, J. W. Hutchinson, and F. W. Zok, "Dynamic shear rupture of steel plates", *Journal of the Mechanics of Materials and Structures* **This issue** (2007).

[Needleman and Tvergaard 1994] A. Needleman and T. Tvergaard, "Mesh effects in the analysis of dynamic ductile crack growth", *Eng. Fract. Mech.* **47** (1994), 75–91.

[Nurick and Shave 2000] G. N. Nurick and G. C. Shave, "The deformation and tearing of thin square plates subjected to impulsive loads- an experimental study", *Int. J. Mech. Sci.* **18** (2000), 99–116.

[Radford et al. 2005] D. D. Radford, N. A. Fleck, and V. S. Deshpande, "The response of clamped sandwich beams subjected to shock loading", *Int. J. Impact Eng.* **32** (2005), 968–987.

[Rathbun et al. 2006] H. J. Rathbun, D. D. Radford, Z. Xue, M. Y. He, J. Yang, V. S. Deshpande, N. A. Fleck, J. W. Hutchinson, F. W. Zok, and A. G. Evans, "Performance of metallic honeycomb-core sandwich beams under shock loading", *Int. J. Solids Struct.* **43** (2006), 1746–1763.

[Taylor 1941] G. I. Taylor, "The pressure and impulse of submarine explosion waves on plates", pp. 287–303 in *The scientific papers of G. I. Taylor*, vol. III, Cambridge University Press, 1963, 1941.

[Wang and Hopkins 1954] A. J. Wang and H. G. Hopkins, "On the plastic deformation of built-in circular plates under impulsive load", *J. Mech. Phys. Solids* **3** (1954), 22–37.

[Xue and Hutchinson 2003] Z. Xue and J. W. Hutchinson, "Preliminary assessment of sandwich plates subject to blast loads", *Int. J. Mech. Sci.* **45** (2003), 687–705.

SOHRAB KAZEMAHVAZI: sohrabk@kth.se
Cambridge University Engineering Department, Trumpington Street, Cambridge, CB2 1PZ, United Kingdom

DARREN RADFORD: radfordd@aecl.ca
Cambridge University Engineering Department, Trumpington Street, Cambridge, CB2 1PZ, United Kingdom

VIKRAM S. DESHPANDE: vsd@eng.cam.ac.uk
Cambridge University Engineering Department, Trumpington Street, Cambridge, CB2 1PZ, United Kingdom

NORMAN A. FLECK: naf1@eng.cam.ac.uk
Cambridge University Engineering Department, Trumpington Street, Cambridge, CB2 1PZ, United Kingdom